PERIODICO di MINERALOGIA
established in 1930

DIPARTIMENTO
DI SCIENZE DELLA TERRA

SAPIENZA
UNIVERSITÀ DI ROMA

An International Journal of
Mineralogy, Crystallography, Geochemistry,
Ore Deposits, Petrology, Volcanology
and applied topics on Environment, Archaeometry and Cultural Heritage

Evolution of Nb-mineralization in the Chuktukon carbonatite massif, Chadobets upland (Krasnoyarsk Territory, Russia)

Dmitry A. Chebotarev [a,*], Anna G. Doroshkevich [a, b], Reiner Klemd [c], Nikolay S. Karmanov [a]

[a] V.S. Sobolev Institute of Geology and Mineralogy, Siberian Branch of Russian Academy of Sciences, pr. Akad Koptyuga, 3, Novosibirsk, 630090, Russia
[b] Geological Institute SB RAS, Ulan-Ude, Sakhyanovoy Str., 6a, 670047, Russia
[c] Friedrich-Alexander-Universität Erlangen-Nürnberg, Germany

ARTICLE INFO

Submitted: June 2017
Accepted: June 2017
Available on line: August 2017

* Corresponding author:
chebotarev@igm.nsc.ru

DOI: 10.2451/2017PM733

How to cite this article:
Chebotarev D.A. et al. (2017)
Period. Mineral. 86, 99-118

ABSTRACT

This paper reports on new study of the niobium mineralization of the Chuktukon carbonatites and weathering crust. The Chuktukon massif is located within the Chadobets upland in the southwestern part of the Siberian Platform. Primary Nb-minerals of carbonatites are pyrochlore group minerals (mainly fluorcalciopyrochlore), newly discovered mineral - rippite $[K_2(Nb,Ti)_2(Si_4O_{12})O(O,F)]$, and Nb-rutile. Fluorcalciopyrochlore has oscillatory zonation with variations in content of Nb_2O_5 (59-67 wt%), TiO_2 (2.8-5 wt%), SiO_2 (up to 3.3 wt%), CaO (15.9-17.7 wt%), Na_2O (7-8.2 wt%) and F (4.5-5.13 wt%). Rippite is Nb-rich silicate (~44 wt% of Nb_2O_5) and contains inclusions of primary fluorcalciopyrochlore. Nb-rutile form oscillatory and sectorial hourglass-like zoned crystals with variable content of Nb_2O_5 (9-14.7 wt%). The carbonatites underwent strong hydrothermal alteration and subsequent weathering, and, as a result, in the hydrothermally altered carbonatites and weathering crust the primary Nb-minerals become unstable, dissolve and decompose, and Nb-bearing goethite (up to 4.3 wt% of Nb_2O_5) formed. Primary fluorcalciopyrochlore is replaced by the secondary Sr-, Pb-, LREE- and Ba-rich pyrochlore group minerals.

Keywords: pyrochlore; rippite; rutile; goethite; carbonatite; carbonatite deposit; weathering crust; Krasnoyarsk territory; niobium.

INTRODUCTION

Niobium is a relatively rare lithophile transition metal. It is a strategically important metal, which is in wide use. It is very useful in the industry because doping with small amounts of niobium greatly improves the yield strength, weldability, corrosion and heat resistance of steel. Therefore, it is used in the manufacturing of high-strength low-alloy steels, superalloys for the jet and rocket engine components, corrosion and heat-resistant alloys. The Nb-based alloys and compounds are used as superconductors, superconductor magnets and electroceramics. Because of these useful properties, the worldwide mine production of niobium for the last 20 years was increased by more than 3.5 times (USGS, 1997, 2016). The element is concentrated to potentially mineable levels in carbonatites and alkaline silicate igneous rocks and their weathering products, for example, the Araxá and Catalão lateritic profile over carbonatites and phoscorites in Brazil, the Lovozero nepheline syenites in Russia, and others.

The bulk of global production of niobium comes from pyrochlore supergroup minerals and, to a lesser degree, from columbite-group minerals and loparite. Herewith, the Brazilian laterites over carbonatite complexes (Araxá and Catalão) yielded about 92% of worldwide production (Mitchell, 2015). The Chuktukon carbonatites and weathering crust upon them may considered as key

world objects in the production of niobium. The economic reserves of the deposit is 39.8 Mt at 0.6 wt% of Nb_2O_5 (Lomayev and Serdyuk, 2011). The technological features and main Nb minerals of the Chuktukon ores are described in details (Slukin, 1994; Tsykina, 2004). The author concluded that the main Nb minerals in carbonatites and weathering crust are primary and secondary pyrochlores.

Detailed knowledge of the trace element composition of carbonatite minerals is essential for constraining the distribution of Nb, REE and other rare metals in mineralized carbonatites of potential economic value. Several recent studies have investigated the trace element distribution between rock-forming minerals in carbonatites, but the data collection is still in its early stages. So far, Xu et al. (2010, 2015), Reguir et al. (2012), Chen and Simonetti (2012), Chakhmouradian et al. (2016 a,b, 2017) reported information about trace element composition of rock-forming minerals, such as apatite, carbonates, clinopyroxene and amphibole-group minerals, which is useful for understanding of mechanisms of Nb and REE enrichment and the economic potential of carbonatites.

In this study, we present new data on the Nb mineralization of the Chuktukon carbonatites and weathering crust and trace element composition of Nb minerals, and interpret these data in the context of processes of Nb distribution during the evolution of the Chuktukon system. Our investigations revealed that in addition to pyrochlore, considerable amounts of Nb contained in the newly discovered mineral rippite (potassium niobium silicate) (Sharygin et al., 2016 a,b; Doroshkevich et al., 2016 a,b; Chebotarev et al., 2016) from some species of primary carbonatites and in the goethite formed in the hydrothermally altered carbonatites and weathering crust.

GEOLOGIC BACKGROUND AND SHORT DESCRIPTION OF CARBONATITES AND WEATHERING CRUST

The Chuktukon massif is part of the structure of the Chadobets upland located on the southwestern margin of the Siberian Platform and represents one of the Platform areas of alkaline-ultramafic magmatic formation. The Chadobets upland has the ellipse-like shape with axes of 45 and 35 km (Figure 1). There are two ledges forming the upland core: the northern (Terinovskiy) and the southern (Chuktukon). Neoproterozoic and Cambrian sedimentary rocks are exposed in the core and at the periphery of the complex, respectively. These are slates, siltsones, sandstones, dolomites, pebbles, and coal interlays. The external frame of the upland is composed of Permian-Carboniferous and Lower Triassic tuffs and fields of subhorizontal Lower Triassic traps. Magmatic rocks of the Chuktukon massif are presented by the ultramafic alkaline rocks (melilitite-nepheline and pyroxene peridotites, picrite, melteigite), carbonatite and kimberlite; the sequence of rocks (from the earliest to the latest) comprises ultramafic alkaline rocks (picrites), carbonatites and kimberlites, post-dating carbonatites (Slukin, 1994; Lapin, 1997, 2001; Lapin and Lisitsyn, 2004; Kirichenko et al., 2012). The ages of the picrites and carbonatites are 252±12 (U-Pb sensitive high mass-resolution ion microprobe II (SHRIMP II) on perovskite) and 231±2.7 Ma (Ar-Ar on rippite), respectively (Chebotarev et al., 2017).

Carbonatites of the Chuktukon massif form several stock-like carbonatite bodies of 1.2x0.7 km in size as well as dykes and sills of carbonatites with different thicknesses in Proterozoic sediments (Slukin, 1994; Lapin, 1997, 2001; Lapin and Lisitsyn, 2004; Kirichenko et al., 2012). Hydrothermal processes were intense following the initial crystallization of carbonatite, resulting in the formation of hydrothermally altered areas of the rocks.

Natural exposure of the magmatic rocks is extremely poor because sedimentary rocks and thick weathering crust cover the rocks. The general structure of the weathering crust upon carbonatites has been described by Slukin (1994) and Tsykina (2004). The weathering crust outcrops extend over an area of approximately 16 km^2. The lower part of the weathering profile (disintegration zone) consists of moderately weathered carbonatites. The rocks often leached along a net of fissures. The thickness of this zone is up to 260 meters. Amount of REE_2O_3, Nb_2O_5 and P_2O_5 in the disintegration zone is up to 6 wt%, 1.3 wt% and 14 wt%, respectively. The structure of the disintegration zone is complicated by intense hydrothermally altered areas of the carbonatites. Highly weathered rocks in the upper part of the profile are ochres. The thickness of ochre zone is up to 100 m. The ochres contain lenses and layers of "iron-stones" up to 5-15 m thick. The ochres are rich in REE_2O_3 (up to 25 wt%), Nb_2O_5 (up to 5 wt%) and P_2O_5 (up to 23 wt%). The borders between different levels of weathering crust are very variable, and weathering features can be found even deeper than 460 m. The age of the weathering crust is 102.6±2.9 Ma (U-Pb SHRIMP II on monazite) (Chebotarev et al., 2017).

PETROGRAPHY OF CARBONATITE ROCKS

The carbonatites are fine- and medium-grained and have white and brown colour and different shades with massive, spotty and less frequently banded textures (Figure 2 a,b,c). Mineral composition of carbonatites and weathering crust is presented in Table 1. The main primary mineral is calcite; the minor and accessory primary minerals are dolomite, strontianite, pyrochlore group minerals, Nb-rutile, rippite, fluorapatite, pyrite, tainiolite, ancylite-(Ce), K-feldspar and quartz-1 (Chebotarev, 2016; Chebotarev et al., 2016, 2017; Doroshkevich et al., 2016 a,b; Sharygin et al., 2016 a,b). The weak to very intensive hydrothermal

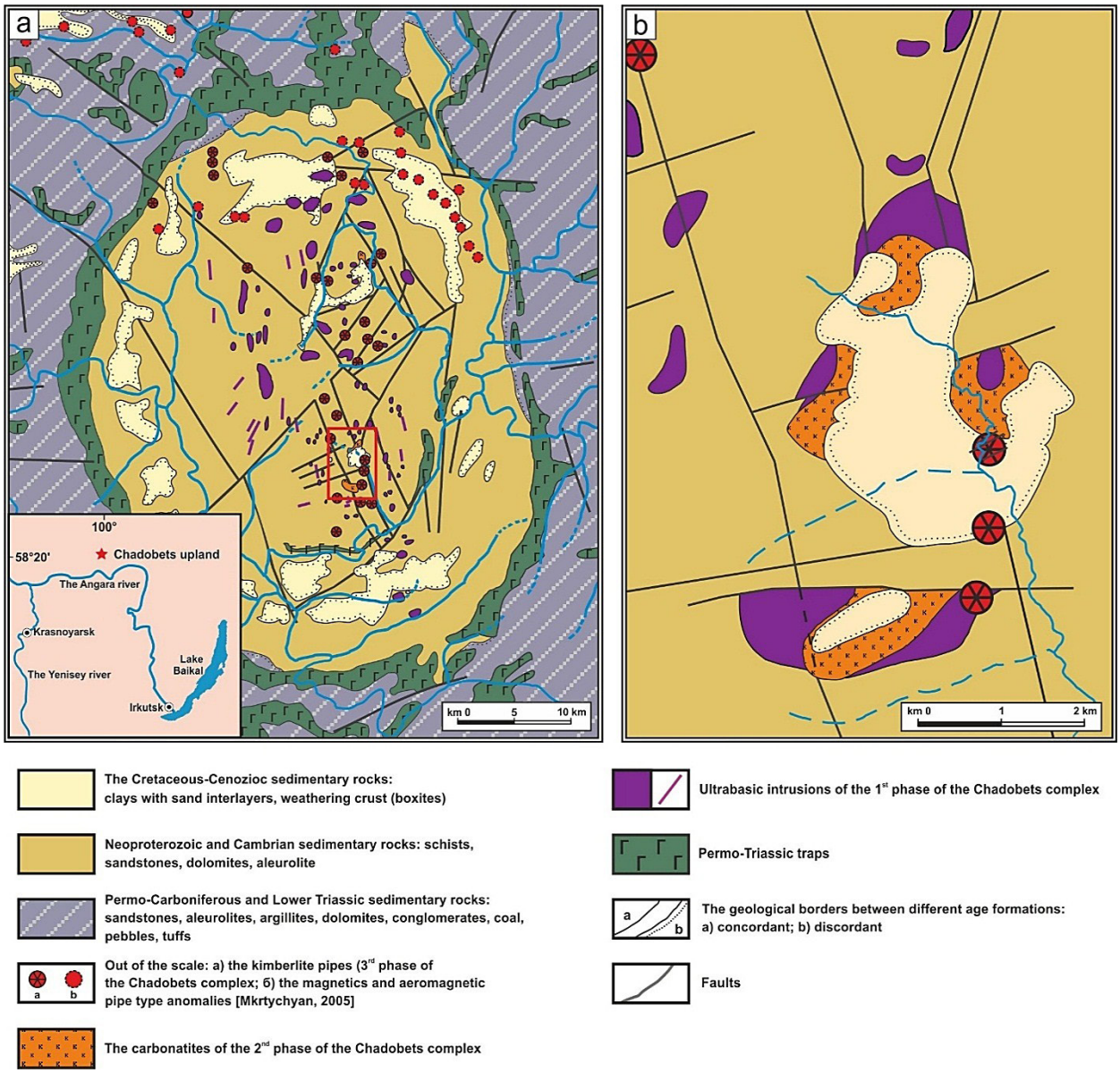

Figure 1. Simplified geologic map of the Chadobets upland (a) and the Chuktukon carbonatite massif (b) after Kirichenko et al. (2012).

alteration led to the formation of quartz-2, barite, goethite, psilomelane (romanechite±hollandite), Ba-Sr-pyrochlore group minerals, parisite-(Ce), synchysite-(Ce), monazite-(Ce), carbonate-rich fluorapatite, aegirine interstitially among grains of primary minerals (Figures 3 a,b,c,d, 8, 9, 10 a,b,c,d,e,f,g). Burbankite, strontianite, daqingshanite-(Ce), ferrohagendorfite, unidentified Na-REE-Ba-Sr-Ca-rich phosphates occasionally occur in secondary inclusions in fluorapatite and calcite (Sharygin et al., 2016a). In the weathering crust upon carbonatites, goethite, florencite-(Ce), psilomelane, kaolinite and monazite-(Ce) are the main minerals (Figure 10 h,i,j,k). Churchite-(Y), zircon and rutile occur as accessory minerals in the weathering crust. The product of the weathering crust are brown and dark brown ochres with relicts of carbonatite (Figure 2 d,e).

METHODS

Since the carbonatites are overlapped by a thick weathering crust, the study of the rocks is possible only by drilling methods and samples of rocks were core fragments. Thin sections were prepared from the core fragments and separated mineral monofraction of pyrochlore was placed in epoxy resin and polished by diamond pastes, using pure alcohol.

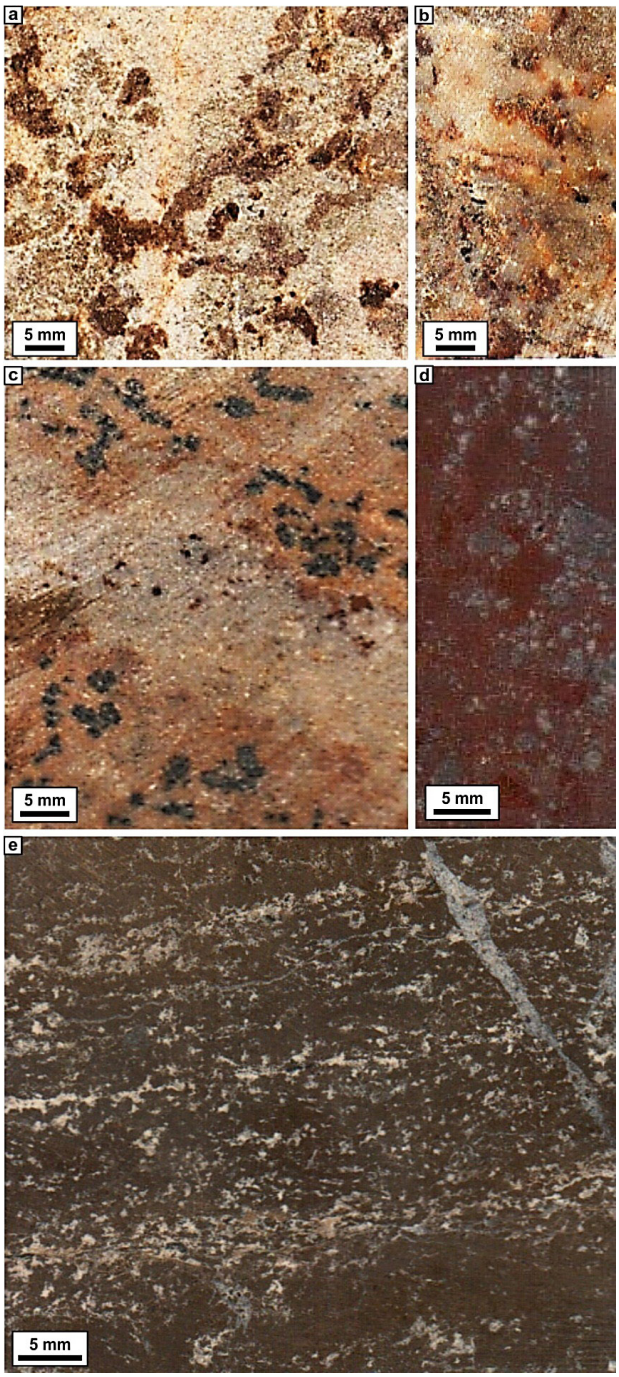

Figure 2. Photos of textural features of the rocks of the Chuktukon carbonatite massif. a, b, c – hydrothermally altered carbonatites; d, e – the weathering crust upon carbonatites.

Rock textures and mineral assemblages were studied using an optical petrographic microscope and energy-dispersive spectrometry (EDS) in combination with back-scattered electron imaging (BSE) using a MIRA 3LMU SEM (TESCAN Ltd.) equipped with an INCA Energy 450 XMax 80 microanalysis system (Oxford Instruments Ltd.) in the Analytical Center for multi-elemental and isotope research SB RAS (Novosibirsk, Russia). The samples were coated with a 25 μm conductive carbon coating. EDS analyses were made at low vacuum of 60-80 Pa, an accelerating voltage of 20 kV, a probe current of 1 nA, and accumulation time of 20 s. The simple compounds and metals were used as reference samples for most of the elements: SiO_2 (Si-Kα and O-Kα), diopside (Mg-Kα and Ca-Kα), albite (Na-Kα), orthoclase (K-Kα), $Ca_2P_2O_7$ (P-Kα), BaF_2 (Ba-Kα and F-Kα), pyrite (S-Kα), SrF_2 (Sr-Kα), Ti (Ti-Kα), V (V-Kα), Fe (Fe-Kα), Mn (Mn-Kα), Zn (Zn-Kα), Zr (Zr-Lα), Nb (Nb-Lα), various (LREE)PO_4 (LREE-Lα), UO_2 (U-Mα). Correction for matrix effects was made by the XPP algorithm, implemented in the software of the microanalysis system. Metallic Co served for quantitative optimization (normalization to probe current and energy calibration of the spectrometer).

Electron microprobe analyses (EMPA) with wavelength-dispersive spectrometry (WDS) were made at the same Analytical center using the «CAMEBAX-micro» electron microprobe. The operating conditions were chosen to minimize devolatilization: beam diameter of 1-2 μm, accelerating voltage of 20 kV and a beam current of 15–25 nA, counting time of 5 s for Na and Fe, 10 s for F, Nb, Ti, Si, K, Ca, Nd, Zr, U, Pr, Th, Ce, Sr, Pb, La, Ba and 20 s for Y. Data reduction was performed using a PAP routine (Pichou and Pichoir, 1984). The received BSE-images were used to select appropriate points for quantitative electron microprobe analyses. The following standards were used for quantification of the elements: diopside (Si-Kα, Ca-Kα), albite (Na-Kα), fluorphlogopite (F-Kα, K-Kα), synthetic $LiNbO_3$-REE (Nb-Lα), TiO_2 (Ti-Kα), Fe_2O_3 (Fe-Kα), $NdPO_4$ (Nd-Lα), zircon (Zr-Lα), $PrPO_4$ (Pr-Lα), UPO_4 (U-Mα), YPO_4 (Y-Lα), ThO_2 (Th-Mα), $CePO_4$ (Ce-Lβ), $Pb_2P_2O_7$ (Pb-Mα), $LaPO_4$ (La-Lα), Sr-glass (Sr-Lα), Ba-glass (Ba-Lα). Relative standard deviation was less 2%.

Trace element analyses by LA-ICP-MS for minerals were performed with thin-sections (using an ESI New Wave UP193FX laser ablation accessory coupled to an Agilent Technologies 7500i ICP-MS at the Friedrich-Alexander-Universität Erlangen-Nürnberg (Erlangen, Germany). The ICP-MS operated with a plasma power of 1350 W, while He (0.65 l/min) and Ar (1.10 l/min) were used as carrier gases. Furthermore, Ar acted as plasma (14.9 l/min) and auxiliary gas (0.9 l/min). Laser fluence was 2.7 J/cm^2 and repetition rate 16 Hz. Data were calibrated using the NIST SRM 610 glass reference material for the oxides. Internal standards were natural and synthetic minerals and glasses. Measurements were conducted with a single spot size of 10-50 μm in diameter. In order to check the analytical accuracy, analyses of minor elements in all minerals were compared to the respective microprobe results and, in addition, synthetic minerals were analyzed and used for

Table 1. Mineral composition of carbonatites and weathering crust upon them of the Chuktukon carbonatites.

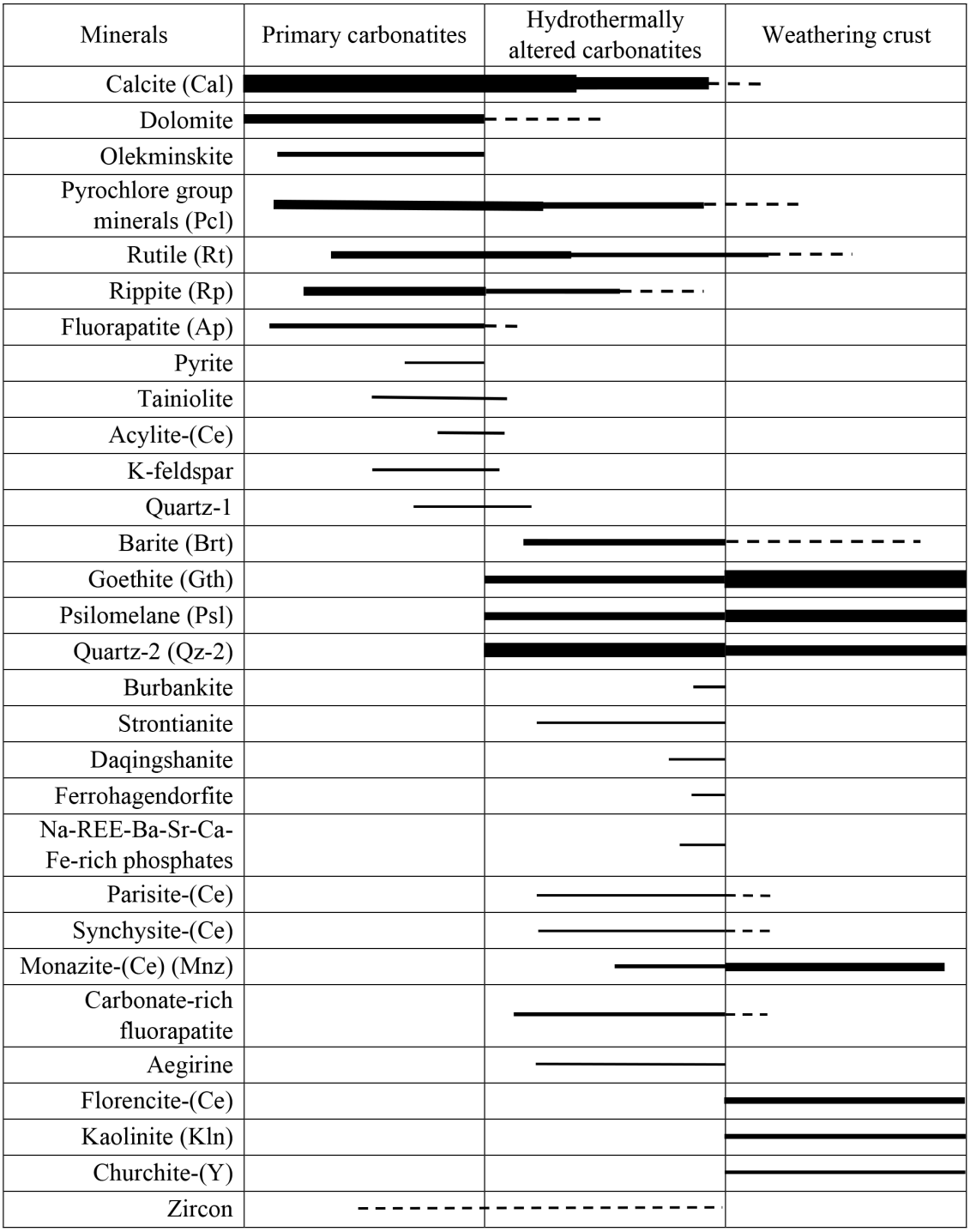

Table was constructed using Tsykina (2004), Sharygin et al. (2016a,b) and author's data.

the comparison of trace elements. The calculation of trace element concentrations was conducted by the GLITTER Version 3.0 on-line interactive data reduction for LA-ICP-MS Program by Macquarie Res. (2000). The 1σ error based on counting statistics from signal and background is <10%. Reproducibility of measurements was checked by repeated analyses of the NIST SRM 610 and 612 glasses and is generally better than 5% relative.

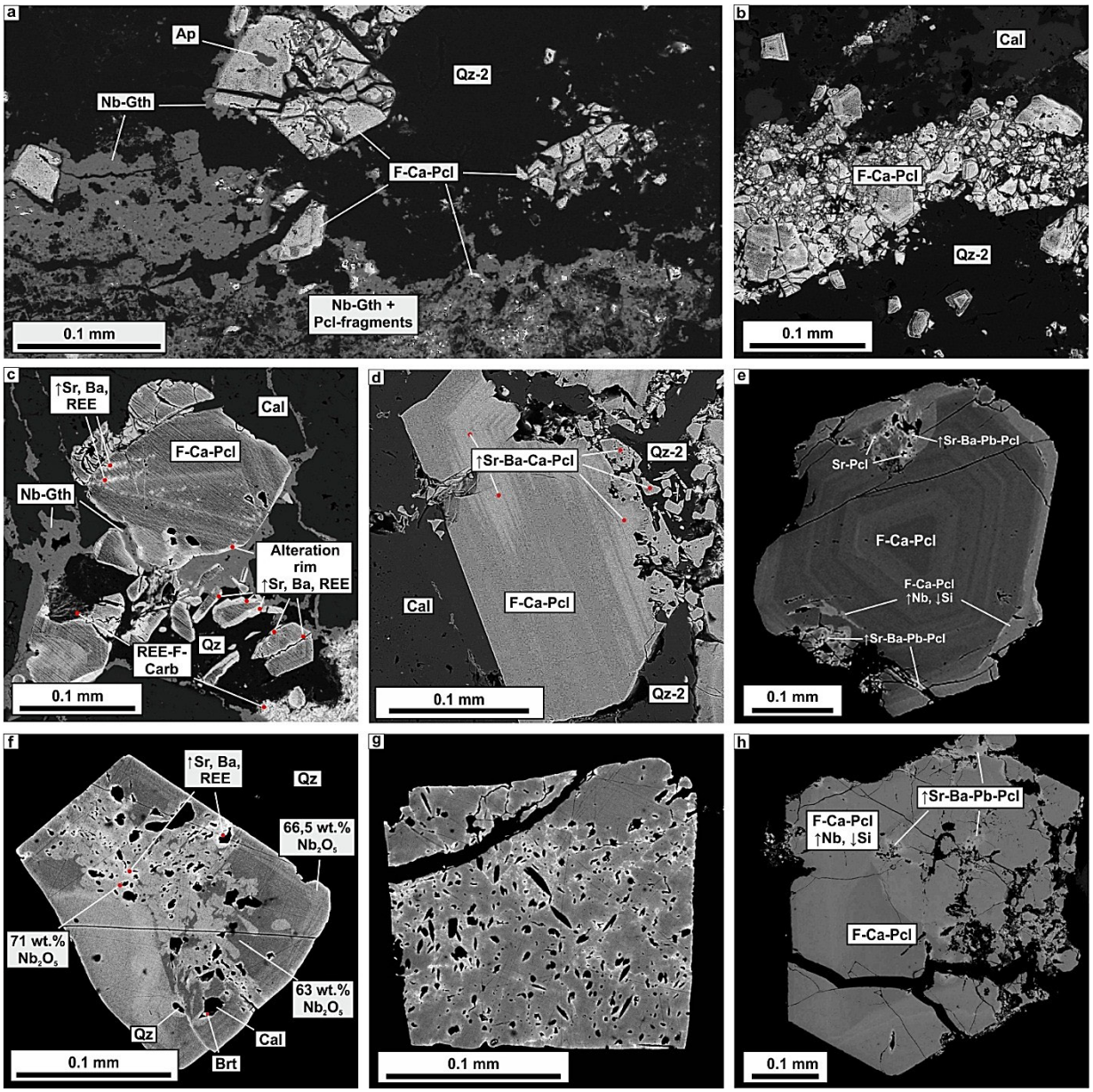

Figure 3. The BSE images of the pyrochlore group minerals from the Chuktukon carbonatite. a, b - Fine-grained irregular shaped fragments of shattered pyrochlore group minerals, forming crystalline aggregates in matrix of the hydrothermally formed Nb-goethite in the quartz veinlet in crushed part of the Chuktukon carbonatite. c – The fragments and parts of the crystals of the pyrochlore group minerals, contacting with the hydrothermal quartz, have an alteration rim and patchy zonation (light shades), unlike the parts, contacting with calcite. d – Decomposing of the pyrochlore crystal, contacting with hydrothermal quarz, while the part in contact with calcite is smoothly faced. e, f, g, h – Strongly altered pyrochlore crystals. Areas along crystal defects are enriched in Sr, Ba, Pb and REE and have lighter shades in BSE. For the abbreviations see Table 1.

NB-MINERALIZATION IN CARBONATITE AND WEATHERING CRUST

The pyrochlore supergroup minerals

The minerals form octahedral light brown, brown to black crystals 0.2-1 mm in size. In the crushed parts of rocks, it forms crystalline aggregates (Figure 3 a,b). The minerals contain primary inclusions of calcite, strontianite, fluorapatite and secondary inclusions of barite and carbonate-rich fluorapatite (Figure 2a) (Chebotarev et al., 2016). It has two types of zonation: oscillatory and patchy, which have bright light shades at BSE-images (Figures 3 b,c,d,e, 4). The patchy zonation might combine within one crystal with oscillatory zonation (Figures 2 c,d, 3).

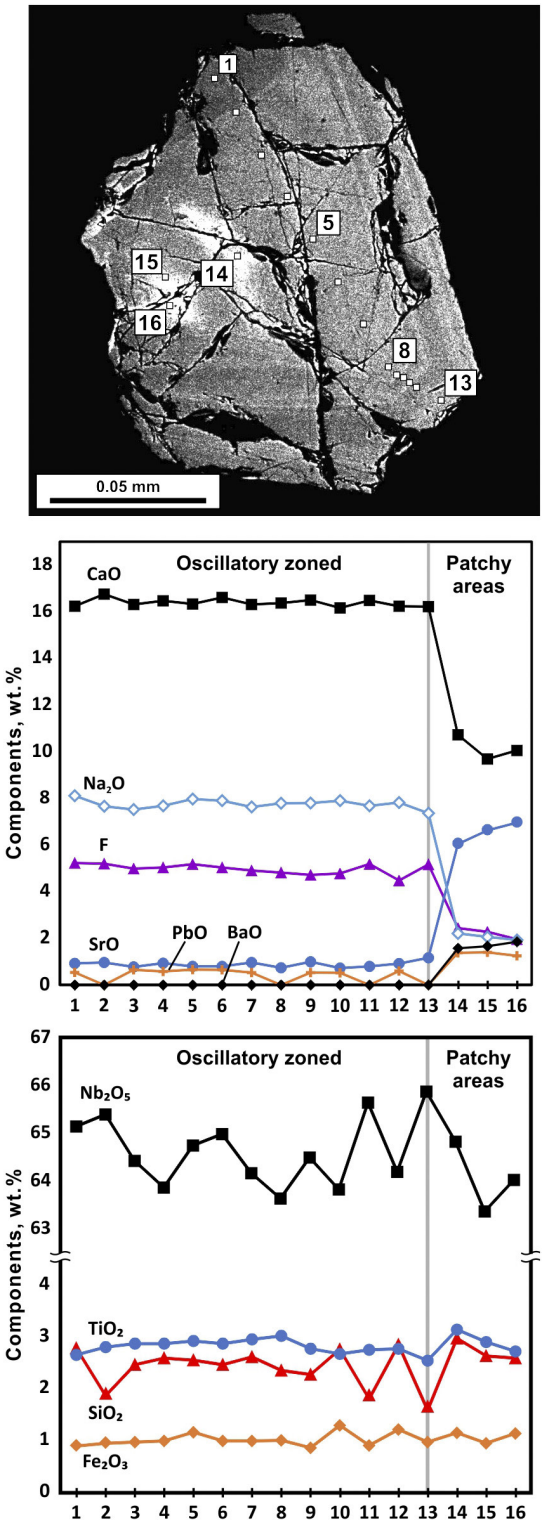

Figure 4. Analyses profile (in wt%) along the hydrothermally altered oscillatory-zoned pyrochlore group mineral from the Chuktukon carbonatite. Large cracks are result of vacuuming procedure in the analytical chamber. Small white squares indicate the places of microprobe analyses.

Crystals contacting hydrothermal quartz have an alteration rim (Figure 3 c,d,e,f,g,h). The patchy zoned pyrochlore is abundant in the hydrothermally altered carbonatites. The patchy zoned areas are confined to the outer crystal parts and crystal defect borders: cracks and weakened areas along the inclusion borders (Figure 3 c,d,e,f,g,h).

The B-site of all the Chuktukon pyrochlore supergroup minerals are generally occupied by Nb, matching the pyrochlore group composition (Hogarth, 1977; Atencio et al., 2010) (Table 2, Figure 5), and occupancy of the A- and Y-sites highly varies (Figure 6).

In crystals with oscillatory zonation, variations in content of Nb_2O_5 (from 59 to 67 wt%), TiO_2 (from 2.8 to 5 wt%), SiO_2 (to 3.3 wt%), CaO (from 15.9 to 17.7 wt%), Na_2O (from 7 to 8.2 wt%) and F (from 4.5 to 5.1 wt%) are observed (Table 2, Figures 4, 6). The amount of elements other than Nb, Ti, Ca and Na is relatively low. The mineral can be classified as fluorcalciopyrochlore (Atencio et al., 2010) or pyrochlore (Hogarth, 1977). The constancy of fluctuations of niobium, titanium and other components means that the oscillation zonation of pyrochlore is related to the rhythmical chemistry variations of the mineral-forming environment during pyrochlore crystallization.

The areas with the patchy zonation are diverse in composition in comparison with the oscillatory-zoned crystals. It is enriched in SrO (up to the 11.4 wt%), BaO (up to 4.6 wt%), PbO (up to 4.2 wt%), and LREE (up to 0.5 wt%) as compared to the oscillatory-zoned crystals (Table 2, 3; Figures 2d, 4, 5). The content of Nb_2O_5 is higher (up to 71 wt%), SiO_2 and TiO_2 are lower (up to 2.5 wt%). The amounts of CaO (from 5.6 to 14 wt%), F (up to 2 wt%) and Na_2O (up to 2.5 wt%) are lower, than in the darker (in BSE images) and oscillatory-zoned areas. Generally, the composition of patchy zoned pyrochlores falls to calico-, strontio- and kenopyrochlore subgroups (Atencio et al., 2010). According to Hogarth (1977), minerals should be classified as pyrochlore and Sr-Ba-Pb-rich pyrochlore. In the weathering crust, the pyrochlores become highly porous (Figure 3 e,f,g,h) and immediately turn to powder at extraction, so the least replaced pyrochlores were analysed.

In addition to Sr-rich pyrochlore obtained by us, the researches (e.g., Slukin, 1994; Tsykina, 2004; Kirichenko et al., 2012) have observed the Ba-, Pb- and Ce-rich pyrochlores in the Chuktukon weathering crust. There are peaks on the X-ray pictures of the average Chuktukon ores, corresponding to Ba- and Sr-rich minerals of pyrochlore supergroup (Tsykina, 2004). According to the calculations, based on chemical composition of weathering crust, carried out by V. Vlasov and A. Lapin, the content of the minerals of pyrochlore supergroup in the average mineral composition of the ores is 1.65% (Tsykina, 2004). Also, Tsykina (2004) revealed a strong positive correlation between the contents of iron and

Table 2. Representative analyses of pyrochlore.

	Primary pyrochlores						Altered pyrochlores						
	Fluorcalcipyrochlore						Strontiopyrochlore			Sr-rich calciopyrochlore		Calciopyrochlore	
Sample no.	1	2	3	4	5	6	7	8	9	10	11	12	13
Na_2O, wt%	7.43	6.94	6.97	6.66	6.83	6.66	0.69	0.86	0.77	1.11	0.98	2.02	1.62
CaO	16.03	16.45	16.35	17.43	16.33	17.43	4.89	5.05	3.26	6.78	5.57	15.51	10.56
SrO	0.84	0.90	0.84	0.67	1.02	0.65	11.46	10.57	11.44	9.67	9.00	2.01	6.27
BaO	-	-	-	-	-	-	2.65	2.63	1.36	2.39	4.59	0.02	1.34
PbO	-	-	-	-	-	-	-	-	1.47	-	4.16	-	-
La_2O_3	0.04	0.03	0.05	0.07	0.01	0.08	0.37	0.28	0.48	0.25	-	0.17	0.18
Ce_2O_3	0.06	0.10	0.13	0.16	0.07	0.27	0.09	0.15	1.27	0.12	-	0.07	0.13
Nd_2O_3	0.05	0.05	0.03	0.03	0.02	0.07	-	0.02	0.03	-	-	0.04	0.03
Pr_2O_3	0.03	-	0.02	-	-	0.03	0.07	0.04	0.09	0.08	-	0.01	0.02
ThO_2	-	-	0.03	0.07	0.01	0.22	-	0.03	0.14	0.03	-	-	0.02
UO_2	0.14	0.08	0.06	0.04	0.02	0.01	0.16	0.21	0.87	0.14	-	0.30	0.16
SiO_2	3.15	1.55	2.02	0.02	0.01	-	2.97	3.33	1.65	3.14	1.97	0.12	3.30
TiO_2	3.04	2.57	2.60	3.59	3.28	4.41	3.03	3.15	3.56	3.21	6.69	2.89	3.23
ZrO_2	2.01	1.67	1.97	0.19	0.04	0.57	1.98	1.89	0.09	2.01	-	0.12	1.92
Fe_2O_3	1.31	0.82	0.97	1.00	0.07	0.28	1.12	1.34	3.61	1.20	1.15	0.79	1.31
Nb_2O_5	61.17	63.62	62.90	64.57	67.26	64.47	60.06	60.10	57.99	61.36	54.38	69.93	60.85
Ta_2O_5	-	0.10	0.07	0.02	0.05	0.09	-	0.07	0.25	0.06	-	0.10	0.09
F	4.73	5.04	4.81	5.28	4.82	4.81	1.44	1.47	2.82	1.82	1.65	1.82	1.95
K_2O	0.17	0.10	0.12	0.02	0.05	0.04	0.07	0.12	0.27	0.11	0.42	0.04	0.16
Total	100.18	100.01	99.94	99.82	99.88	100.07	91.05	91.31	91.42	93.47	90.56	95.96	93.13
Formulae based on 2 B-site cations, a.p.f.u.													
Na	0.822	0.798	0.792	0.788	0.803	0.783	0.078	0.096	0.089	0.122	0.114	0.226	0.179
Ca	0.980	1.046	1.027	1.140	1.061	1.133	0.306	0.311	0.209	0.413	0.358	0.961	0.643
Sr	0.028	0.031	0.029	0.024	0.036	0.023	0.388	0.352	0.398	0.319	0.313	0.067	0.207
Ba	0.000	0.000	0.000	0.000	0.000	0.000	0.061	0.059	0.032	0.053	0.108	0.000	0.030
Pb	0.000	0.000	0.000	0.000	0.000	0.000	0.000	0.000	0.024	0.000	0.067	0.000	0.000
La	0.001	0.001	0.001	0.002	0.000	0.002	0.008	0.006	0.011	0.005	0.000	0.004	0.004
Nd	0.001	0.001	0.001	0.001	0.000	0.001	0.000	0.000	0.001	0.000	0.000	0.001	0.001
Pr	0.001	0.000	0.000	0.000	0.000	0.001	0.001	0.001	0.002	0.002	0.000	0.000	0.000
Ce	0.001	0.002	0.003	0.004	0.002	0.006	0.002	0.003	0.027	0.002	0.000	0.001	0.003
Th	0.000	0.000	0.001	0.002	0.000	0.006	0.000	0.001	0.004	0.001	0.000	0.000	0.001
U	0.003	0.002	0.002	0.001	0.001	0.000	0.004	0.005	0.023	0.004	0.000	0.008	0.004
Site A	1.836	1.881	1.855	1.961	1.904	1.954	0.849	0.834	0.819	0.921	0.961	1.269	1.070
Si	0.180	0.092	0.118	0.001	0.000	0.000	0.174	0.191	0.099	0.178	0.118	0.007	0.188
Ti	0.130	0.115	0.115	0.165	0.150	0.201	0.133	0.136	0.160	0.137	0.302	0.126	0.138
Zr	0.056	0.048	0.056	0.006	0.001	0.017	0.056	0.053	0.003	0.056	0.000	0.003	0.053
Fe^{3+}	0.056	0.037	0.043	0.046	0.003	0.013	0.049	0.058	0.163	0.051	0.103	0.034	0.056
Nb	1.578	1.707	1.667	1.782	1.845	1.768	1.587	1.561	1.571	1.576	1.476	1.828	1.564
Ta	0.000	0.002	0.001	0.000	0.001	0.001	0.000	0.001	0.004	0.001	0.000	0.002	0.001
Site B	2.000	2.000	2.000	2.000	2.000	2.000	2.000	2.000	2.000	2.000	2.000	2.000	2.000
F	0.853	0.946	0.892	1.019	0.925	0.923	0.266	0.267	0.535	0.327	0.313	0.333	0.351
K	0.012	0.008	0.009	0.002	0.004	0.003	0.005	0.009	0.021	0.008	0.032	0.003	0.011
Site Y	0.866	0.953	0.900	1.021	0.928	0.926	0.271	0.276	0.555	0.335	0.345	0.336	0.362

Fe^{3+} was calculated by stoichiometry.

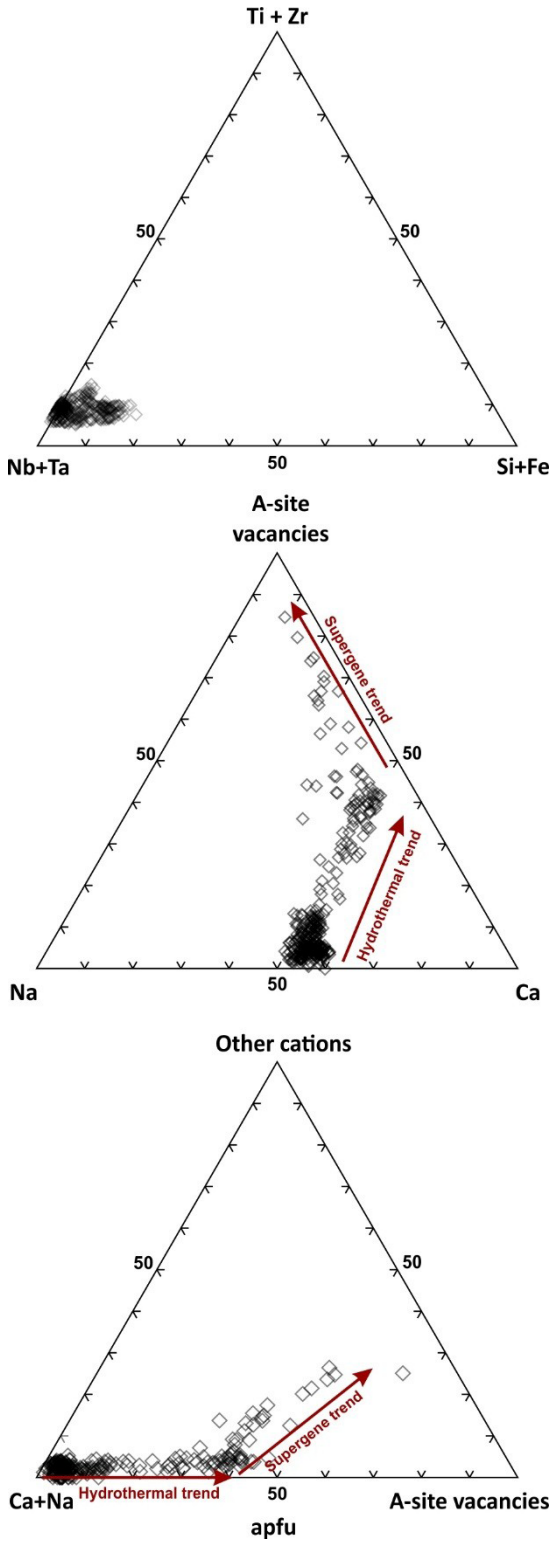

Figure 5. Compositional variations of B- and A-cations (apfu) of the pyrochlore group minerals from the Chuktukon carbonatites. Hydrothermal trend – substitution of Na and F by A- and Y-site vacancies, supergene trend – substitution of Ca by A-site vacancies and substitution of A- and Y-site vacancies by A-site cations, such as Sr, Ba, LREE, Pb.

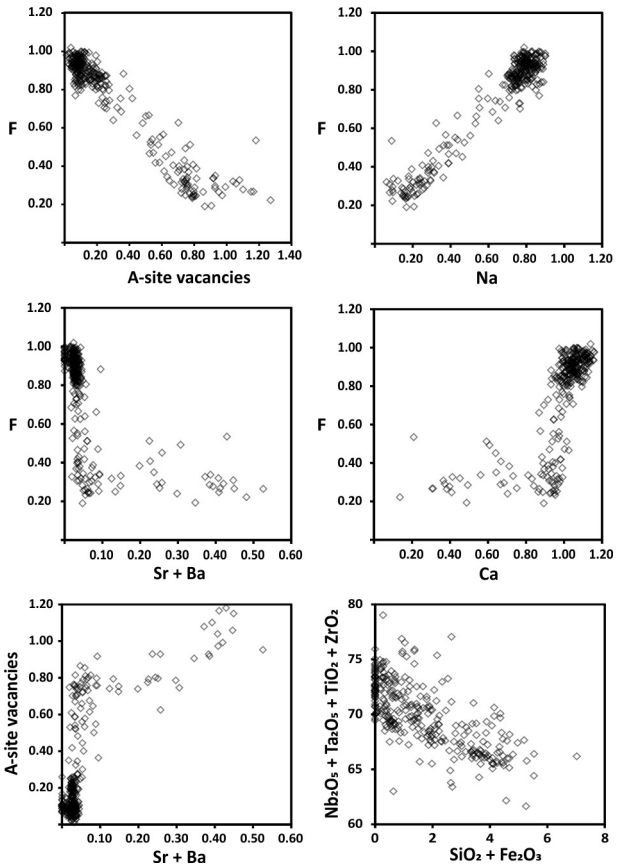

Figure 6. Compositional variations of A-cations (apfu) and B-cations (wt%) of the pyrochlore group minerals from the Chuktukon carbonatite.

niobium. According to our observations, the minerals of the pyrochlore supergroup in the weathering crust are much less common than by the calculations of V. Vlasov and A. Lapin, but due to the revealed correlation, we conclude that niobium is concentrated in the structure of other supergene minerals, mostly in goethite.

All pyrochlore types show similar chondrite-normalized REE patterns and strongly enriched LREE with La_{cn}/Lu_{cn} ratios 160-770 (Table 3, Figure 7). There is, however, much variation in the absolute REE concentrations. Pyrochlore with patchy zonation has a generally high REE concentration, whereas minerals with oscillatory zonation have a lower REE range. A slightly positive Ce anomaly [$Ce/Ce^*=Ce_{cn}/0.5*(La_{cn}+Pr_{cn})$=1.35-1.60] occurs in the REE plots of patchy-zoned pyrochlores instead Ce/Ce*=1.08-1.14 of other pyrochlores. The researchers associate the positive anomaly with the oxidation of Ce^{3+} to Ce^{4+} due to changes in fO_2 by fluctuations of the water table (Mariano, 1989 a,b; Willet et al., 1989; Möller, 2000; Nasraoui and Bilal, 2000).

Table 3. Concentration of trace elements in pyrochlore.

	Unaltered pyrochlore					Altered pyrochlore			
wt%	1	2			3	4		5	
CaO	16.78	17.03	17.28	17.42	16.72	17.24	16.99	17.41	16.85
Na_2O	6.99	7.05	7.02	6.70	7.05	6.87	7.08	6.92	7.12
SiO_2	1.82	1.95	1.60	1.00	2.12	-	-	0.30	1.01
TiO_2	3.62	3.64	3.59	3.79	3.44	4.28	4.09	4.01	4.92
Fe_2O_3	1.14	1.29	0.94	0.54	1.07	-	-	1.20	1.25
Nb_2O_5	64.42	65.05	65.22	65.99	64.13	66.08	67.54	65.42	62.89
F	4.68	4.60	4.61	4.42	4.62	4.88	5.17	4.94	5.16
K_2O	0.37	-	-	-	-	-	-	-	-
Total	99.81	100.60	100.26	99.86	99.15	99.34	100.86	100.19	99.21
Li, ppm	0.93	2.81	1.31	2	0.97	-	-	0.52	0.67
P	43	27	18	22	24	15	24	26	41
Sc	2.09	2.31	1.87	2.03	2.1	3.06	2.34	5.45	5.97
V	212	212	195	203	179	34	28.2	66.7	67.3
Mn	181	176	115	129	141	45.7	66.5	80.5	63.2
Co	0.08	0.04	0.06	0.05	0.05	0.05	0.06	0.04	0.06
Ga	5.8	6.9	4.8	5.3	4.8	2.1	9.8	3.6	16.8
Sr	5622	5628	5768	5804	5550	4476	4800	4415	4888
Y	7.93	7.62	6.74	7.38	7.03	29.8	33.1	26.7	34.6
Zr	3187	3418	3144	3274	3518	5669	4060	9079	10341
Ba	111	142	93	106	97	31	192	70	373
La	233	244	278	264	222	738	885	697	868
Ce	463	483	581	555	442	2484	2925	1976	2337
Pr	39	40	47	44	37	183	215	154	182
Nd	109	112	128	121	103	543	634	450	548
Sm	12	12	14	13	11	64	74	51	62
Eu	3.02	2.84	3.38	3.19	2.59	15.4	16.9	12.7	14.8
Gd	6.16	5.62	6.66	6.66	5.53	29.5	34.6	23.8	31.3
Tb	0.54	0.47	0.56	0.55	0.42	2.79	3.15	2.3	3.13
Dy	2.03	2.03	2.11	2.21	1.85	11.7	13.4	9.86	13.2
Ho	0.26	0.28	0.26	0.27	0.24	1.38	1.67	1.17	1.59
Er	0.70	0.73	0.55	0.69	0.62	3.02	3.44	2.21	3.46
Tm	0.11	0.1	0.07	0.09	0.08	0.3	0.3	0.27	0.34
Yb	0.97	0.9	0.71	0.69	0.76	1.3	1.55	1.39	1.71
Lu	0.15	0.16	0.1	0.1	0.08	0.13	0.13	0.09	0.17
Hf	3.56	3.25	2.8	2.91	3.36	32.2	28.3	43.5	55.3
Ta	6.96	4.32	2.55	3.31	2.29	3.99	33.4	5.83	34.7
Th	88.7	92.7	90.1	93.7	72.2	579	658	416	511
U	18	30.5	16.5	23.6	9.6	0.2	4.9	1.3	7.4

Rippite

Rippite was firstly discovered in the Chuktukon massif (Doroshkevich et al., 2016, Sharygin et al., 2016). It was found as a primary mineral in some hydrothermally altered carbonatites. Mineral forms colourless prismatic crystals (up to 0.5-2 mm) in the carbonate matrix (Figure 8). It contains primary inclusions of pyrochlore (with a composition close to the oscillation-zoned pyrochlore crystals), calcite

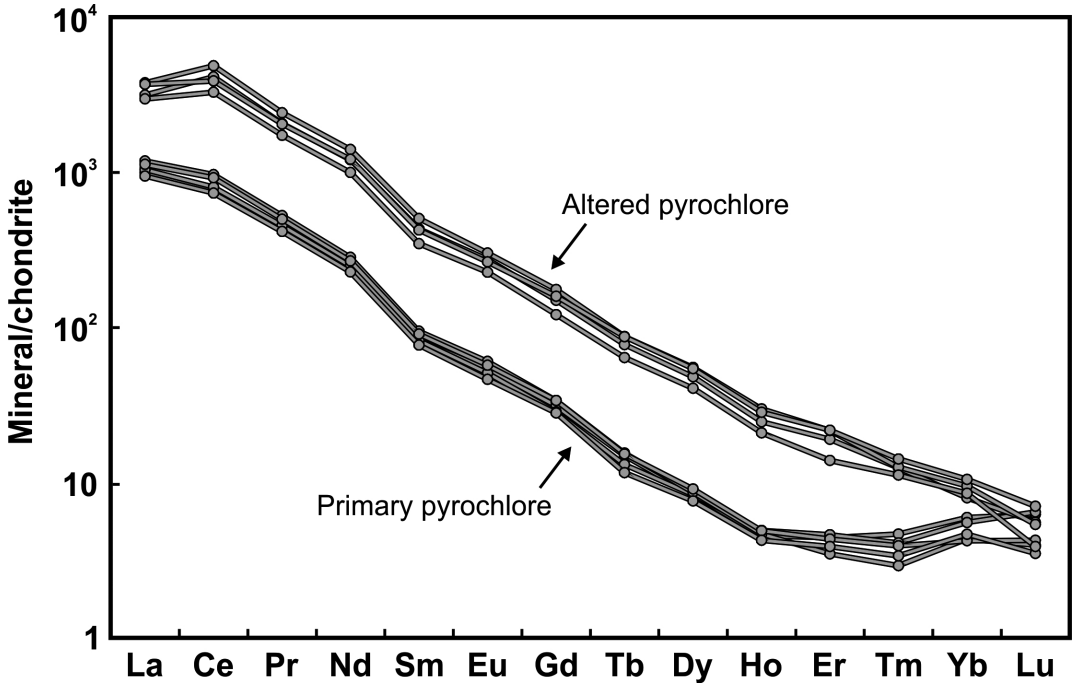

Figure 7. Chondrite-normalized REE plot for pyrochlore. Normalizing value for chondrite is from Sun and McDonough (1989).

and secondary inclusions of barite and quartz. Inclusions of pyrochlore in the rippite crystals indicate that rippite originated later, than pyrochlore. In the hydrothermally altered carbonatites, most of the crystals become unstable and are overgrown at grain edges and cleavage planes by quartz, associated with barite and goethite (Figure 9).

Rippite is structurally related to cyclosilicates with $[Si_4O_{12}]^{8-}$ 4-membered single rings with the simplified formula $K_2(Nb,Ti)_2(Si_4O_{12})O(O,F)$ (Doroshkevich et al., 2016, Sharygin et al., 2016). Most of the crystals are unzoned or weakly-zoned and have chemical compositions with low amounts of TiO_2 (up to 0.7 wt%) (Table 4). Only a few grains have a narrow rims with a high Ti content (up to 4.4 wt% of TiO_2). The REE and trace element concentrations in rippite are consistently low (<220 ppm) (Table 4).

It is interesting to note that the mineral with proportion of the main components (K:Nb:Si) similar to rippite has been described in carbonatite of the Araxá complex, Brazil (Traversa et al., 2001). The authors identified the mineral as nenadkevichite (labuntsovite group) due to a low total sum of analyse. Apparently, further studies allow determining whether this mineral is rippite or it is vuoriyarvite-K (labuntsovite group).

Rutile

Rutile is accessory mineral and forms crystals up to tenths of mm in size and crystalline aggregates in crushed parts of carbonatites (Figure 8). The crystals have oscillatory and sectorial hourglass-like zonation in TiO_2, Nb_2O_5 and FeO distribution (Table 5, Figure 9). The crystals that contacted with the hydrothermally altered areas of rocks have rim, enriched in Nb_2O_5 up to 17 wt% (Figure 9). According to the stoichiometry, the type of substitutions in the rutile appears to be $3Ti^{4+} \leftrightarrow Fe^{2+}+2Nb^{5+}$.

There are many descriptions of Nb-rutile in carbonatites. For example, it is found in Vuorviarvi and Kangaduba intrusions at the Veseloe and Kola peninsula carbonatites (Bulakh et al., 2000; Pilipiuk et al., 2001; Doroshkevich et al., 2007b) and with brookite in the Salpeterkop complex, South Africa (Verwoerd et al., 1995). Although rutile and its polymorph brookite do not occur in large quantities in carbonatites, they do form hydrothermal deposits associated with carbonatite complexes, e.g., at Magnet Cove, USA, which is the locality for large brookite crystals (Verwoerd et al., 1995). Apparently, Nb incorporates to rutile at the magmatic stage of the carbonatites evolution and can be redistributed by hydrothermal fluids, as it takes place with the Chuktukon rutile enriched in niobium during the hydrothermal process.

In the strongly hydrothermally altered areas and in the weathering crust, rutile presents the slightly corroded crystals (Figure 9). Mineral from the weathering crust has lower concentrations of V, Fe and Nb than in the primary and hydrothermally altered carbonatites (Table 5).

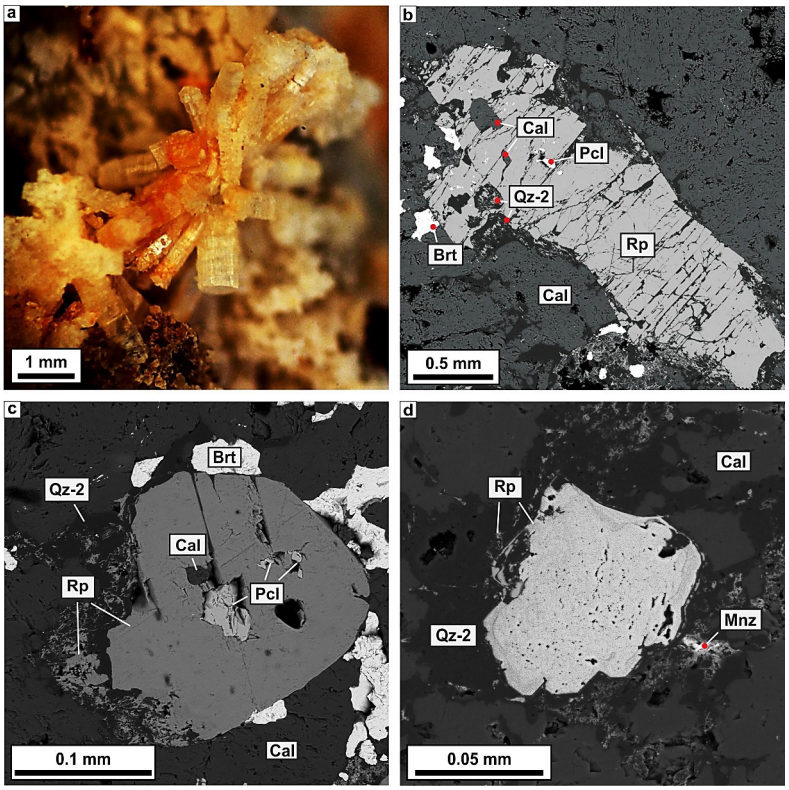

Figure 8. The rippite crystals from the Chuktukon carbonatite. a – The photo of radial-radiant aggregate of the rippite crystals in pickled carbonatite. b – The rippite crystal in the quartz-calcite matrix in BSE. c, d – Decomposition of the rippite crystals, contacting with late quartz in BSE.

Goethite

There are Nb-free and Nb-bearing varieties of goethite in the carbonatites of the Chuktukon massif and weathering crust upon carbonatites (Table 6). The mineral forms the pseudomorphoses after some undetectable primary minerals and pyrite, the massive fine-grained and banded aggregates in the hydrothermally altered carbonatites and in the weathering crust (Figure 10). In the hydrothermally altered carbonatites, the mineral occurs in veinlets with quartz, psilomelane, barite and Ca-REE-fluorcarbonates (Figure 3 a,c, 10 a,b,d). In the weathering crust, mineral associates with kaolinite, monazite and florencite-(Ce) (Figure 10 h,i,j,k).

Nb-bearing goethite from the hydrothermally altered carbonatites contains up to 2.2 wt% of Nb_2O_5 (0.9 in average) and is distinguished by higher contents of SiO_2 (up to 6.6 wt%), ZnO (up to 1.2 wt%) and V_2O_3 (up to 1.3 wt%). Goethite that fully replaced the primary minerals in the hydrothermally altered carbonatites usually has higher content of FeO (76.8 wt% in average), admixtures of Al_2O_3, SiO_2, Nb_2O_5 is below detection limit (Table 6).

Goethite from weathering crust is Nb-bearing and there are two species of the mineral. Goethite from the ochres is in groundmass in association with kaolinite and compose fragments. The nature of the fragments is uncertain. It might be fully replaced by Nb-goethite fragments of primary minerals, but on the other hand, some of the fragments have striated texture and might be fragments of the goethitized carbonatites or goethite, originated at hydrothermal alteration stage (Figure 10 h, i). The fragments have higher contents of FeO (81.8 wt% in average), Nb_2O_5 (1.5 wt% in average), Al_2O_3 (up to 1.7 wt%) and lower content of SiO_2 (up to 1.6 wt%) as compared to Nb-goethite from hydrothermally altered carbonatites. Nb-goethite from groundmass have even more higher content of Nb_2O_3 (up to 4.3 wt%, 1.8 wt% in average), Al_2O_3 (up to 7 wt%), TiO_2 (up to 5.5 wt%), and P_2O_5 (up to 3.9 wt%) in comparison with the mineral from the hydrothermally altered carbonatites and fragments, but lower content of FeO (76 wt% in average) than in fragments (Table 6, Figure 11).

Another specie of Nb-goethite is in disintegration zone. It forms groundmass in association with florencite-(Ce) and monazite (Figure 10 j,k). It has highest content of Nb_2O_5 (up to 4 wt%), while the contents of other components are slightly different from those of Nb-goethite from hydrothermally altered carbonatites, with the exception of SiO_2, whose content is 1.2 wt%.

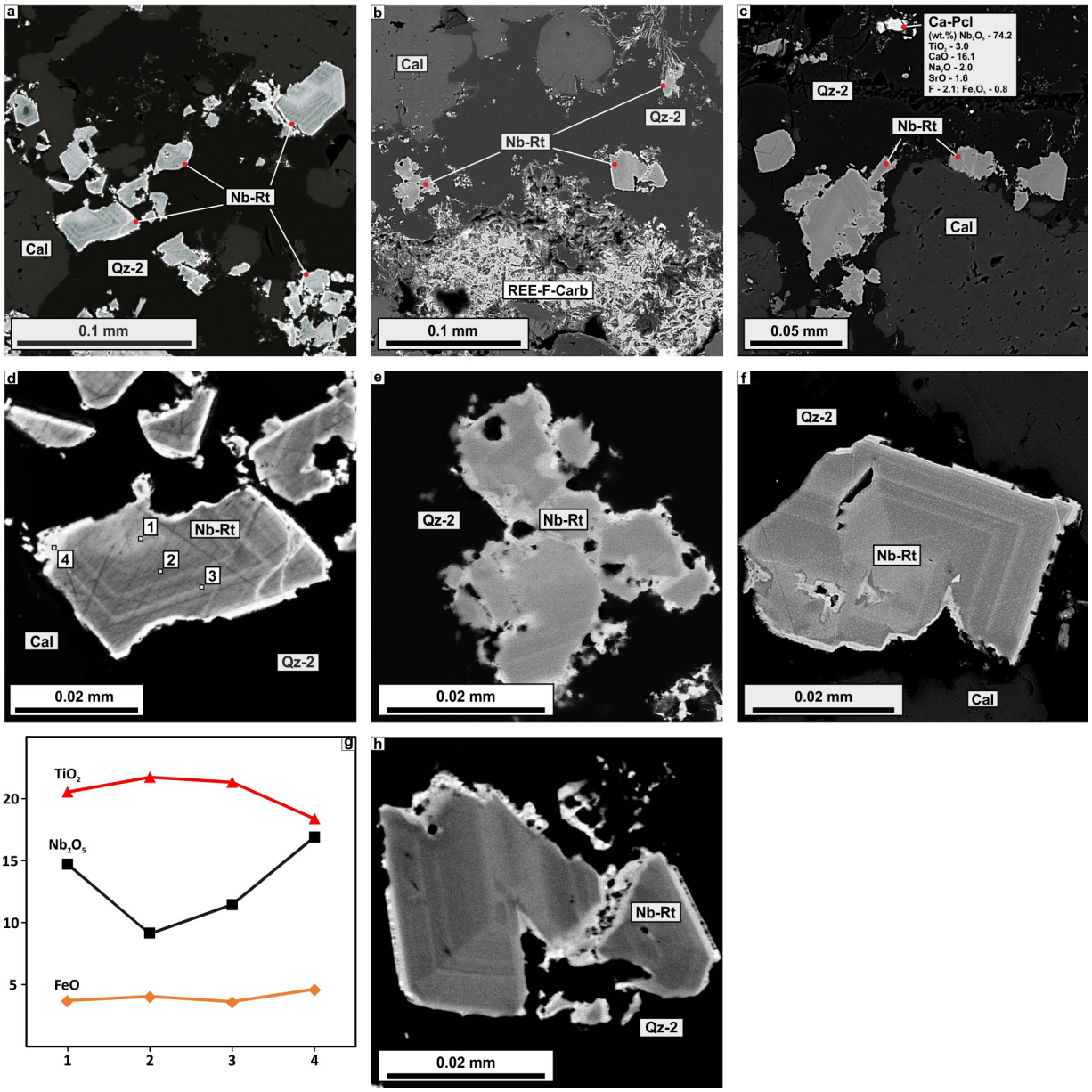

Figure 9. The BSE-images of Nb-rutile from the hydrothermally altered Chuktukon carbonatite. a, b, c – Shattered zoned Nb-rutile in quartz veinlet. d, e, f, h – Resorbed oscillatory and hourglass-like zoned Nb-rutile crystals with enriched in Nb rim in quartz veinlet. g – Analysis profile for rutile crystal from d (TiO_2 content is decreased by 4 times, Table 5). For the abbreviations see Table 1.

The presence of Nb in composition of goethite (up to 14 wt% of Nb_2O_5) has been described in only few natural systems, such as in weathering crust in Lueshe, Congo (Wall et al., 1996). Authors have concluded that the Nb can incorporate into the goethite structure. Furthermore, goethite with amounts of Nb up to 0.3 a.p.f.u. was synthesized at low temperatures by Oliveira et al. (2007, 2008, 2010), that proves that Nb-goethite can originate during supergene and low-temperature hydrothermal processes. On one side, the goethite that formed pseudomorphoses after the primary Nb-minerals can inherit the element. On the other side, Nb-goethite aggregates from the matrix look fairly homogeneous and there are no tiny inclusions of Nb-minerals (e.g., pyrochlore), observed even at maximum magnification (taking into account our BSE-images). In addition, Tsykina (2004) has determined strong linear correlation between Fe and Nb in the Chuktukon weathering crust.

Table 4. The representative analyses of rippite.

wt%	1	2	3	4	5	6	7	8
SiO_2	40.88	40.73	40.24	40.39	40.78	40.09	40.86	40.35
TiO_2	0.72	0.57	0.85	0.80	1.80	1.02	0.55	0.35
Nb_2O_5	42.86	42.9	43.25	43.99	42.14	43.57	43.85	45.03
K_2O	15.02	15.11	15.01	15.32	15.20	15.05	15.30	15.11
Total	99.48	99.31	99.35	100.50	99.92	99.73	100.56	100.84
P, ppm	23.6	20.2	25.4	20.9	-	-	-	-
Sc	7.23	6.92	8.68	10.20	-	-	-	-
Ti	4211	4317	2438	3171	-	-	-	-
Ga	1.42	1.79	0.63	0.49	-	-	-	-
Sr	1.08	1.54	0.45	0.94	-	-	-	-
Y	0.09	0.06	0.06	0.13	-	-	-	-
Ba	211	191	126	180	-	-	-	-
La	0.08	0.02	0.02	0.09	-	-	-	-
Ce	0.13	0.03	0.05	0.14	-	-	-	-
Pr	-	0.01	-	0.02	-	-	-	-
Nd	-	-	0.07	-	-	-	-	-
Eu	0.03	-	-	-	-	-	-	-
Yb	0.07	-	0.05	0.01	-	-	-	-
Hf	23.3	20.2	16.1	55.2	-	-	-	-
Ta	7.10	7.45	9.67	12.90	-	-	-	-
Th	0.08	0.02	0.05	0.15	-	-	-	-
U	0.61	0.60	0.28	0.42	-	-	-	-

Table 5. The representative analyses of Nb-rutile from the Chuktukon carbonatite.

wt%	Hydrothermally altered carbonatites									Weathering crust
	1	2	3	4	5	Core 1	2	3	Rim 4	1
TiO_2	79.88	86.51	81.53	83.65	82.82	81.2	85.97	84.35	75.56	97.43
SiO_2	0.51	0.17	0.41	0.49	-	-	-	-	0.43	-
CaO	0.36	0.14	0.78	0.52	0.17	0.34	0.27	0.15	1.3	-
FeO	4.44	3.64	4.1	4.22	3.5	3.71	4.05	3.63	4.63	1.84
V_2O_3	-	-	-	-	1.29	0.79	1.1	1.07	1.34	0.37
Nb_2O_5	14.86	9.97	13.55	11.77	12.93	14.73	9.11	11.46	16.92	0.83
Total	100,05	100,43	100,37	100,65	100,71	100,77	100,5	100,66	100,18	100.47

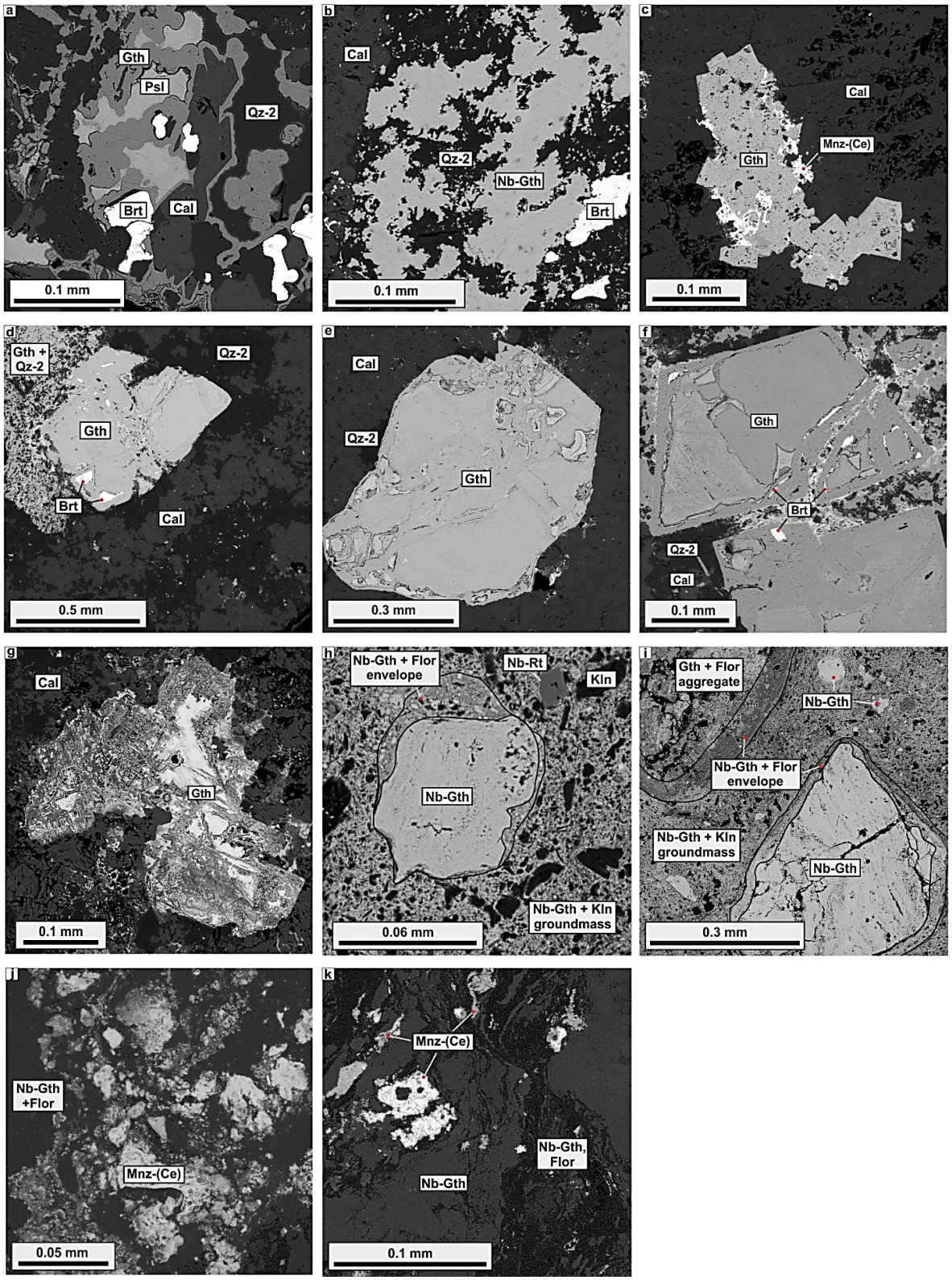

Figure 10. The morphology of goethite from the Chuktukon carbonatite massif. a, b – Goethite in association with quarz-2, barite and REE-fluorcarbonates in hydrothermally altered carbonatites. c, d, e, f – Pseudomorphoses upon pyrite in hydrothermally altered carbonatites. g – Pseudomorphoses upon undetectable mineral in hydrothermally altered carbonatites. h, i – Goethite from the ochres of weathering crust. j, k – Goethite from the disintegration zone of the weathering crust.

Table 6. Representative analyses of goethite from the hydrothermally altered carbonatites and weathering crust upon carbonatites from the Chuktukon carbonatite massif.

		wt%	FeO	Nb_2O_5	TiO_2	Al_2O_3	SiO_2	CaO	MgO	ZnO	V_2O_3	MnO	P_2O_5	SO_3	Total
Hydrothermally altered carbonatites	In association with quarz-2, barite, REE-F-Carb	1	65.90	0.93	0.90	0.76	6.6	0.3	0.4	-	0.28	-	-	-	76.00
		2	66.4	0.67	-	-	5.4	0.5	-	0.59	0.40	-	-	-	73.92
		3	66.8	1.26		-	3.6	0.9	0.9	-	0.22	-	-	-	73.86
		4	72.8	0.50	0.68	-	2.5	0.6	-	-	-	2.71	-	-	79.71
		5	70.4	2.22	0.63	-	3.7	0.4	0.6	-	-	-	-	-	77.97
		6	65.0	0.69	-	-	6.0	0.5	0.4	-	-	-	0.82	-	73.38
		7	82.3	0.56	-	-	1.2	1.3	-	-	-	-	-	-	85.59
		8	67.7	1.03	0.43	0.77	4.5	0.8	0.9	1.17	0.43	-	-	-	77.71
		9	73.4	0.33	0.65	0.21	3.9	0.2	-	-	1.21	-	-	-	79.84
		10	72.5	0.49	0.97		3.8	0.3	-	-	1.29	-	-	-	79.27
		Avg	**70.3**	**0.87**	**0.71**	**0.58**	**4.1**	**0.6**	**0.6**	**0.88**	**0.64**	**2.71**	**0.82**	**-**	**77.76**
	Pseudomorphoses upon pyrite	1	76.3	-	-	-	2.8	0.2	-	-	-	-	-	-	79.27
		2	74.2	-	-	-	2.8	0.4	1.0	-	-	0.48	-	-	78.81
		3	67.1	-	-	0.62	5.6	0.7	1.5	0.71	0.31	0.41	-	-	76.88
		4	80.9	-	-	-	1.7	1.2	-	-	-	0.35	-	0.45	84.56
		5	75.5	-	-	-	2.9	-	-	-	-	-	-	-	78.32
		6	86.3	-	-	-	1.2	-	-	-	-	-	-	0.60	88.00
		7	76.2	-	-	-	2.6	-	-	-	-	-	-	-	78.73
		8	81.5	-	-	-	2.7	-	-	-	-	-	-	-	84.13
		9	73.1	-	-	-	4.0	-	0.7	-	-	-	-	-	77.75
		Avg	**76.8**	**-**	**-**	**0.62**	**2.9**	**0.6**	**1.0**	**0.71**	**0.31**	**0.41**	**-**	**0.53**	**80.72**
	Pseudomorphoses upon undetectable mineral	1	75.4	-	-	-	2.9	0.9	-	-	-	-	-	0.37	79.63
		2	75.0	-	-	-	2.9	0.8	-	-	-	-	-	-	78.67
		3	79.3	-	-	-	1.8	0.5	-	-	-	-	-	0.35	81.97
		4	75.4	-	0.30	-	3.2	0.5	-	-	-	0.59	-	0.22	80.21
		Avg	**76.3**	**-**	**0.30**	**-**	**2.7**	**0.7**	**-**	**-**	**-**	**0.59**	**-**	**0.31**	**80.12**
Weathering crust, ochres	Fragments	1	89.2		0.35	-	-	-	-	-	-	-	-	-	89.58
		2	87.8	-	0.55	-	0.6	-	-	-	-	-	-	-	88.97
		3	87.8	-	0.30	0.62	-	-	-	-	0.72	-	-	-	89.49
		4	81.8	-	0.50	1.83	2.2	-	-	-	-	-	-	-	86.38
		5	81.3	0.97	0.77	1.49	0.9	0.0	-	-	0.25	2.92	-	-	89.20
		6	75.6	1.86	1.72	2.78	1.2	0.2	-	-	0.43	2.56	-	-	87.40
		7	77.6	1.47	1.13	2.61	1.7	0.1	-	-	0.31	1.69	-	-	87.34
		8	80.4	1.89	0.98	2.83	1.0	-	-	-	0.32	1.64	-	-	89.73
		9	79.5	0.77	0.93	1.66	1.9	-	-	-	0.62	2.03	-	-	87.83
		10	76.5	2.03	1.58	3.10	1.2	-	-	-	0.34	2.54	-	-	88.50
		Avg	**81.8**	**1.50**	**0.88**	**2.12**	**1.3**	**0.1**	**-**	**-**	**0.43**	**2.23**	**-**	**-**	**88.44**
	Groundmass	1	82.1	0.62	0.58	1.89	2.2	-	-	-	0.40	-	-	-	87.75
		2	71.0	-	5.39	5.54	5.5	-	-	-	0.38	0.28	0.53	-	88.63
		3	77.6	-	0.27	4.02	3.1	-	-	-	0.40	-	0.94	-	86.37
		4	80.0	1.36	1.43	1.78	1.4	-	-	-	0.44	1.68	0.55	-	88.67
		5	68.8	4.29	2.84	5.56	-	0.5	-	-	-	1.20	3.23	-	86.46
		6	67.8	1.86	1.05	6.97	0.9	0.5	-	-	-	0.80	3.87	-	83.68
		7	79.4	1.60	0.82	2.04	1.8	-	-	-	0.32	0.58	0.89	-	87.48
		8	72.6	1.62	0.93	4.59	1.9	-	-	-	-	0.67	2.2	-	84.55
		9	78.2	-	0.53	3.97	3.1	-	-	-	-	-	-	-	85.84
		10	81.9	1.09	0.72	2.36	1.6	-	-	-	0.29	-	0.53	-	88.49
		Avg	**76.0**	**1.78**	**1.46**	**3.87**	**2.4**	**0.5**	**-**	**-**	**0.32**	**0.74**	**1.59**	**-**	**86.79**
Weathering crust, disintegration zone		1	71.7	2.26	1.07	0.43	1.3	-	-	0.90	-	-	0.37	-	78.05
		2	70.9	2.40	1.47	0.55	1.2	-	-	0.93	0.21	-	0.76	-	78.43
		3	72.0	2.78	1.10	0.45	1.2	-	-	-	0.21	-	0.50	-	78.25
		4	71.4	3.68	1.02	0.74	1.2	-	-	0.95	0.32	-	-	-	79.29
		5	71.3	3.30	1.13	0.7	1.1	-	-	0.71	0.57	0.35	-	-	79.12
		6	70.8	4.03	1.90	0.55	1.1	-	-	0.55	0.40	0.74	-	-	80.05
		Avg	**71.3**	**3.08**	**1.28**	**0.57**	**1.2**	**-**	**-**	**0.81**	**0.29**	**0.36**	**0.54**	**-**	**78.87**

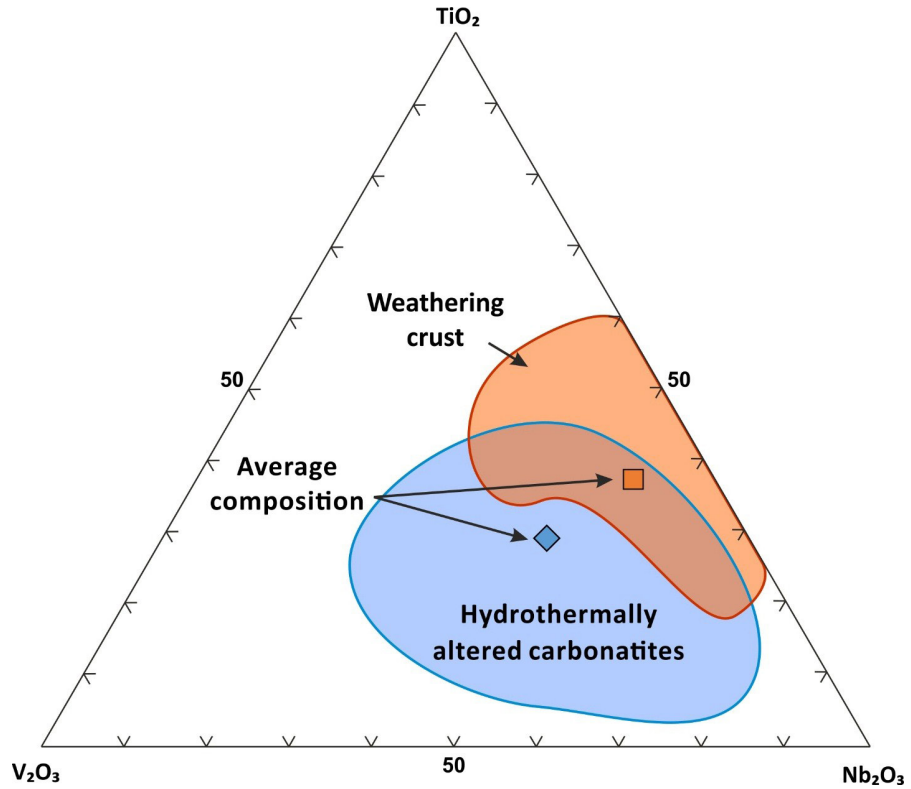

Figure 11. Compositional variations (wt%) of the Nb-rich goethite from hydrothermally altered carbonatites and weathering crust upon carbonatites from the Chuktukon carbonatite massif.

DISCUSSION

The assemblage of niobium minerals changed during the evolution of the Chuktukon system. In primary carbonatites, Nb is in fluorcalciopyrochlore, rippite and rutile. It is important to note, that, in some species of carbonatites, rippite is abundant mineral and it becomes an important concentrator of niobium with pyrochlore.

In hydrothermally altered carbonatites, Nb-goethite and Nb-rich rutile appears, and primary magmatic early-formed pyrochlore replaced along fractures by hydrothermal Sr-, Ba-, Pb-, LREE-rich pyrochlore (Figure 3, 4). The result of replacement can be respresented by the following substitution reactions (Figure 5):

$Na + F^- \rightarrow VA + VY$ (hydrothermal trend)

$Ca + O \rightarrow VA + VY$; $VA + VY \rightarrow A^{2+}$, REE + O, H_2O, OH^- (supergene trend)

where A^{2+} - A-site cation (Sr, Ba, etc), VA and VY are A- and Y-site vacancies, respectively.

The pyrochlore transformation is summarized by the following equation (Nasraoui and Bilal, 2000):

$$3H^+_{(aq)} + H_2O_{(aq)} + [NaCaNb_2O_6F]_{(s)} = [\square_2Nb_2O_5\square 2H_2O]_{(s)} + Na^+_{(aq)} + Ca^{2+}_{(aq)} + HF_{(aq)}$$

The described alteration trends are common to the most of carbonatitic pyrochlores worldwide (Lumpkin and Ewing, 1995). Similar changes have been described in samples from Mabounie, Gabon (Laval et al., 1988); Mt. Weld, Australia (Lottermoser and England, 1988); Tomtor, Russia (Entin et al., 1993); Araxá, Brazil (Lumpkin and Ewing, 1995) and others.

The cation-exchange in pyrochlore is considered to take place at relatively low pH (Nasraoui and Bilal, 2000). Such acidic conditions were probably responsible for the Ca, Fe, REE and F mobility and led to the formation of goethite, carbonate-rich fluorapatite, Ca-REE-fluorcarbonates and monazite-(Ce). In addition, hydrothermal fluid totally dissolves fluorapatite in carbonatites that is evidenced by petrographic observations (the lack of fluorapatite in the hydrothermally altered carbonatites and its presence in pyrochlore as inclusions).

Several experimental data have shown that hydrofluoric acid in fluid also increases the mobility of niobium (Soisson et al., 1961; Bock, 1979; Zaraisky et al., 2010; Linnen et al., 2014; Timofeev et al., 2015). This process

is recorded by the presence of Nb-rich rims in rutile and Nb-goethite in hydrothermally altered carbonatites.

The following supergene alteration of the carbonatites leads to the formation of the weathering crust (ochres) up to 100 m thick enriched in Nb, P, and REE (Slukin, 1994; Tsykina, 2004). The supergene chemical reactions resulted in the dissolution and decomposition of primary minerals and the formation of supergene REE-bearing and Fe-oxide/hydroxide minerals.

Relic primary pyrochlore is eventually subjected to leaching of A-site cations and their replacement at this site by Ba, Sr, LREE and Pb during strong weathering process. Probably, extreme weathering results in ultimately complete decomposition of pyrochlore group minerals and formation of Nb-goethite. A similar process was observed in Seis Lagos, Brazil (Mitchell, 2015) and Mt. Weld, Australia (Lottermoser and England, 1988). Corroded-like form of the rutile crystals in strongly hydrothermally altered areas of carbonatites and in the weathering crust allow us to assume that rutile was partially dissolved or decomposed. It is well known that rutile is a very stable mineral, weakly prone to weathering and forms placer deposits. Nevertheless, experimental data shows that at 240 °C with a mixture of HF and H_2SO_4 components, rutile is completely decompose for 12-16 hours and minerals of pyrochlore, microlite and betafite groups are totally dissolve for 4-8 hours (e.g., Bock, 1979). As far as the authors know, there are no data on the decomposition or dissolution of rippite (or compounds of similar composition), but our petrographic observation suggests, that is possible.

CONCLUSION

The main concentrators of niobium in primary carbonatites of the Chuktukon carbonatite complex are pyrochlore as well as, rippite. Exchange reactions between pyrochlore and hydrothermal fluids possibly occurred at relatively low pH, a_{Na}, $a_{Ca^{2+}}$ and high a_{HF}, $a_{H_2SO_4}$, a_{Sr} and a_{LREE}. The alteration process has been accompained in element redistribution within the pyrochlore crystals, its enrichment in Sr, Ba, REE, Pb, Si with formation of domains of the patchy zonation. Dissolution of the pyrochlore, decomposition of rippite and rutile crystals with formation of Nb-bearing goethite, increasing contents of Nb in the hydrothermally altered rutile indicates that the acid hydrothermal fluids can destroy these minerals and increase the mobility of Nb. Formation of Fe- and Mn-Nb-hydroxides, that are typical for supergene oxidized conditions, indicates that Nb can be remobilized by supergene fluids. It lead to formation of Nb-enriched weathering crust, which may be potentially useful for greater niobium extraction.

ACKNOWLEDGEMENTS

The authors are grateful to the staff of geologists of the "Krasnoyarsk geolsemka" company and personally to A.S. Varganov for providing the collection of core rock samples and his assistance in the preparation of the present work. M.V. Khlestov and E.N. Nigmatullina are thanked for help with EDS- and WDS-analyses at the Analytical Center for multi-elemental and isotope research SB RAS (Novosibirsk, Russia). Helene Brätz is thanked for her assistance with the LA-ICP-MS analyses. The authors thank editor Paolo Ballirano and editoral team for editing and reviewers Jindrich Kynicky and Francesco Stoppa for useful comments and suggestions.

The EDS and EPMA analyses were carried out using funds from and as part of a research project of the Institute of Geology and Mineralogy SB RAS, No 0330-2016-0002, LA-ICP-MS analyses were supported by the Russian Science Foundation (RSF) grant №15-17-20036.

REFERENCES

Atencio D., Andrade M.B., Christy A.G., Giere R., Kartashov M., 2010. The pyrochlore group of minerals: nomenclature. The Canadian Mineralogist 48, 673-698.

Bonyadi Z., Davidson G.J., Mehrabi B., Meffre S., Ghazban F., 2011. Significance of apatite REE depletion and monazite inclusions in the brecciated Se–Chahun iron oxide-apatite deposit, Bafq district, Iran: insights from paragenesis and geochemistry. Chemical Geology 281, 253-269.

Bulakh A.G., Nesterov A.R., Zaitsev A.N., Pilipiuk A.N., Wall F., Kirillov A.S., 2000. Sulfur-containing monazite-(Ce) from late-stage mineral assemblages at the Kandaguba and Vuoriyarvi carbonatite complexes, Kola peninsula, Russia. Neues Jahrbuch fur Mineralogie, Monatshefte 5, 217-233.

Bock R., 1979. A handbook of decomposition methods in analytical chemistry. John Wiley & Sons, Incorporated, 444 pp.

Chakhmouradian A.R., Reguir E., Zaitsev A.N., 2016a. Calcite and dolomite in intrusive carbonatites. I. Textural variations. Mineralogy and Petrology 110, 333-360.

Chakhmouradian A.R., Reguir E., Couëslan C., Yang, 2016b. Calcite and dolomite in intrusive carbonatites. II. Trace-element variations. Mineralogy and Petrology 110, 361-377.

Chakhmouradian A.R., Reguir E.P., A.N. Zaitsev, C. Couëslan, C. Xu, J. Kynický, A.H. Mumin, P. Yang, 2017. Apatite in carbonatitic rocks: Compositional variation, zoning, element partitioning and petrogenetic significance. Lithos 274, 188-213.

Chebotarev D.A., 2016. Compositional and internal structure features of pyrochlores from carbonatites of the Chuktukon carbonatite complex // Moscow International School of Earth Sciences - 2016. Abstracts of International conference. 23-28 May of 2016/ Editor-in-chief L.N. Kogarko. - M.: GEOKHI RAS, 41-42.

Chebotarev D.A., Doroshkevich A.G., SharyginV., 2016. The niobium mineralization in the carbonatites of the Chuktukon

massif, the Chadobets upland (the Krasnoyarsk region, Russia). 33rd International conference «Alkaline Magmatism of the Earth and related strategic metal deposits», Moscow, Russia. Abstracts. 27 may, 2016. Editor-in-chief L.N. Kogarko - M.: GEOKHI RAS, 36. (In Russian).

Chen W. and Simonetti A., 2012. In-situ determination of major and trace elements in calcite and apatite, and U-Pb ages of apatite from the Oka carbonatite complex: insights into a complex crystallization history. Chemical Geology 353, 151-172.

Doroshkevich A.G., Wall F., Ripp G.S., 2007a. Magmatic graphite in dolomite carbonatite at Pogranichnoe, North Transbaikalia, Russia. Contributions to Mineralogy and Petrology 153, 339-353.

Doroshkevich A.G., Wall F., Ripp G.S., 2007b. Calcite-bearing dolomite carbonatite dykes from Veseloe, North Transbaikalia, Russia and possible Cr-rich mantle xenoliths. Mineralogy and Petrology, 90, 19-49.

Doroshkevich A.G., Viladkar S.G., Ripp G.S., Burtseva M.V., 2009. Hydrothermal REE mineralization in the Amba Dongar carbonatite complex, Gujarat, India. The Canadian Mineralogist 47, 1105-1116.

Doroshkevich A.G., SharyginV., Seryotkin Y.V., Karmanov N.S., Belogub E.V., Moroz T.N., Nigmatulina E.N., Eliseev A., Vedenyapin N., Kupriyanov I.N., 2016a. Rippite, IMA 2016-025. CNMNC Newsletter No. 32, August 2016, page 919; Mineralogical Magazine, 80, 915-922.

Doroshkevich, A.G., Chebotarev, D.A., Sharygin,V., 2016b. Alkaline ultrabasic carbonatitic magmatism of the Chadobets upland. // In: Kogarko, L.N. (Ed.): Moscow International School of Earth Sciences - 2016, Moscow (23-28 May 2016), Abstracts, 48-49.

Entin A.R., Yeremenko G.Y., Tyan O.A., 1993. Stages of alteration of primary pyrochlores. Transactions (Dokaldy) of the U.S.S.R. Academy of Sciences: Earth Sciences Sections, 320, 236-239. (Translated from O stadiynosti izmeneniya pervichnykh pirokholorov. Doklady Akademii Nauk SSSR, 1991 319, 1218-1221).

Haggerty S.E., 1991. Oxide mineralogy of the upper mantle. In: Lindsley D.H. (ed.). Oxide Minerals: Petrologic and Magnetic Significance. Mineralogical Society of America. Chantilly, VA, Reviews in mineralogy 25, 355-406.

Harlov D.E., Forster H.J., Nijland T.G., 2002. Fluid-induced nucleation of REE-phosphate minerals in apatite: nature and experiment. Part I. Chlorapatite. American Mineralogist 87, 245-261.

Harlov D.E. and Forster H.J., 2003. Fluid-induced nucleation of REE phosphate minerals in apatite: nature and experiment. Part II. Fluorapatite. American Mineralogist 88, 1209-1229.

Harlov D.E., Wirth R., Forster H.J., 2005. An experimental study of dissolution-reprecipitation in fluorapatite: fluid infiltration and the formation of monazite. Contributions to Mineralogy and Petrology 150, 268-286.

Harlov D.E., 2011. Formation of monazite and xenotime inclusions in fluorapatite megacrysts, Gloserheia Granite Pegmatite, Froland, Bamble Sector, southern Norway. Mineralogy and Petrology 102, 77-86.

Kirichenko T., Zuev K., Perfilova O. Yu., Sosnovskaya O., Smokotina I., Markovich L.A., Borodin, Mironyuk E., 2012. "The state geological map of the Russian Federation. Scale 1:1,000,000 (third generation). Angaro-Eniseysky series. The sheet O-47 - Bratsk. Explanatory note." - SPb.: VSEGEI cartographical factory, 470 pages (163-179). (In Russian).

Knudsen C., 1989. Pyrochlore group minerals from the Qaqarssuk carbonatite complex. Special Publication of the Society for Geology Applied to Mineral Deposits 7 (Lanthanides, Tantalum Niobium), 80-99.

Lapin A.V., 1997. Structure, formation conditions and ore-bearing of the main types of REE in the carvonatite weathering crusts. //Domestic geology 11, 15-22 (In Russian).

Lapin A., 2001. About kimberlites of the Chadobetsky raising in connection with a problem of the formational-metallogeny analysis of the Platform alkaline-ultramain magmatites. // Domestic geology 4, 30-35 (In Russian).

Lapin A., Lisitsyn D., 2004. About a mineralogical typomorphism of alkaline ultramain magmatites of the Chadobetsky raising.// Domestic geology 6, 83-92. (In Russian).

Laval M., Johan V., Tourliere B., 1988. La carbonatite de Mabounie: exemple de formation d'un gite residuel a pyrochlore. Chronique de la Recherche Miniere 491, 125-136.

Li X.C. and Zhou M.F., 2015. Multiple stages of hydrothermal REE remobilization recorded in fluorapatite in the Paleoproterozoic Yinachang Fe-Cu-(REE) deposit, Southwest China. Geochimica et Cosmochimica Acta 166, 53-73.

Linnen R.L., Samson I.M., Williams-Jones A.E., Chakmouradian A.R., in: S.D. Scott (Ed.), 2014. Geochemistry of Rare-Earth Element, Nb, Ta, Hf and Zr Deposits, Treatise on Geochemistry (2nd ed.) 13, 543-568.

Lomayev V.G. and Serdyuk S.S., 2011. The Chuktukon Nb-TR deposit - the priority object for modernization of the Russian rare-earth industry. Journal of Siberian Federal University. Engineering & Technologies 4, 132-154.

Lottermoser B.G. and England B.M., 1988. Compositional variation in pyrochlores from the Mt. Weld Carbonatite laterite, Western Australia. Mineralogy and Petrology 38, 37-51.

Lumpkin G.R. and Ewing R.C., 1995. Geochemical alteration of pyrochlore group minerals: pyrochlore subgrou American Mineralogist 80, 732-743.

Mariano A.N., 1989a. Nature of economic mineralization in carbonatites and related rocks. In: Bell, K. (Ed.), Carbonatite: Genesis and Evolution. Unwin Hyman, London, 149-176.

Mariano A.N., 1989b. Economic Geology of Rare Earth Elements. In: Lipin, B.R., Kay, M. (Eds.), Mineralogical Society of America. Reviews in Mineralogy 21, 309-337.

Möller , 2000. Rare earth elements and yttrium as geochemical

indicators of the source of mineral and thermal waters. In I. Stober and K. Bucher (eds): Hydrology of crystalline rocks. Kluwer Academic Press, 227-246.

Mitchell R.H., 2015. Primary and secondary niobium mineral deposits associated with carbonatites. Ore Geology Reviews, 64, 626-641.

Nasraoui M. and Bilal E., 2000. Pyrochlores from the Lueshe carbonatite complex (Democratic Republic of Congo): a geochemical record of different alteration stages. Journal of Asian Earth Sciences 18, 237-251.

Nasraoui M., 1996. Le gisement de Nobium de Lueshe (Nord Est du Zaire): evolution geochimique et mineralogique d'un complexe carbonatitique en contextes hydrothermale et supergene. // Ph.D. thesis, Ecole des Mines de Paris/Ecole des Mines de Saint Etienne.

Oliveira L.C.A., Gonɜalves M., Oliveira D.Q.L., Guarieiro A.L.N., Pereira M.C., 2007. Synthesis and catalytic properties in oxidation reactions of goethitescontainingniobium. Quimica Nova 30, 925-929.

Oliveira L.C.A., Ramalho T.C., Souza E.F., Gonɜalves M., Oliveira D.Q.L., Pereira M.C., Fabris J.D., 2008. Catalytic properties of goethite prepared in the presence of Nb on oxidation reactions in water: computational and experimental studies. Applied Catalysis B: Environmental 83, 169-176.

Oliveira D.Q.L., Oliveira L.C.A., Murad E., Fabris J.D., Silva A.C., Morais de Menezes, L., 2010. Niobian iron oxides as heterogeneous Fenton catalysts for environmental remediation. Hyperfine Interactions 195, 27-34.

Prokopyev I.R., Doroshkevich A.G., Ponomarchuk A.V., Sergeev S.A., 2017. Mineralogy, age and genesis of apatite-dolomite ores at the Seligdar apatite deposit (Central Aldan, Russia), Ore Geology Reviews 81, 296-308.

Pichou, J.L. and Pichoir, F, 1984. A new model for quantitative X-ray microanalysis. Part I: application to the analysis of homogeneous samples. La Recherche A´erospatiale 3, 13-38.

Pilipiuk A.N., IvanikovV., Bulakh A.G., 2001. Unusual rocks and mineralization in a new carbonatite complex at Kandaguba, Kola Peninsula, Russia. Lithos 56, 333-347.

Reguir E., Chakhmouradian A.R., Pisiak L.K., Halden N.M., Yang , Xu C., Kynicky J., Couëslan C.G., 2012. Trace-element composition and zoning in clinopyroxene- and amphibole-group minerals: implications for element partitioning and evolution of carbonatites. Lithos 128, 27-45.

SharyginV., Doroshkevich A.G., Seryotkin Y.V., Karmanov N.S., Belogub E.V., Moroz T.N, 2016a. A new K-Nb-cyclosilicate $K_2(Nb,Ti)_2(Si_4O_{12})O(O,F)$ from Chuktukon carbonatite massif, Chadobets upland, Russia // 2nd European Mineralogical Conference. Rimini, Italy, 421-421.

SharyginV., Doroshkevich A.G, Chebotarev D.A., 2016b. Na-Sr-Ba-REE-carbonates and phosphates in minerals of Chuktukon massif carbonatites, Chadobets upland, Krasnoyarsk territory // Conference: XVII Russian Fluid Inclusion conference, September 2016, At Ulan-Ude, Russia, 180-182.

Slukin A.D., 1994. Bauxite deposits with unusually high concentrations of REE, Nb, Ti, and Th, Chadobets uplift, Siberian Platform. International Geology Review 36, 179-193.

Soisson D.J., McLafferty J.J., Pierret J.A., 1961. Staff-Industry Collaborative Report: Tantalum and Niobium. Industrial and Engineering Chemistry, 53, 861-868.

Timofeev A., Migdisov Art A., Williams-Jones A.E., 2015. An experimental study of the solubility and speciation of niobium in fluoride-bearing aqueous solutions at elevated temperature. Geochimica et Cosmochimica Acta 158, 103-111.

Tsikyna S.V., 2004. The Nb-REE Chuktukon deposit. Modelling, ore typification and assessment of prospects. // Ph.D. thesis, the Krasnoyarsk Research Institute of Geology and Mineral Resources (In Russian).

U.S. Geological Survey, 1997. Mineral commodity summaries. U.S. Geological Survey, 50-51.

U.S. Geological Survey, 2015. Mineral commodity summaries. U.S. Geological Survey, 116-117.

Verwoerd W.J., Viljoen E.A., Chevallier L., 1995. Rare metal mineralization at the Salpeterkop carbonatite complex, Western Cape Province, South Africa. Journal of African Earth Sciences 21, 171-186.

Wall F., Williams C.T., Woolley A.R., Nasraoui M., 1996. Pyrochlore from weathered carbonatite at Lueshe, Zaire. Mineralogical Magazine 60, 731-750.

Willet G.C., Duncan R.K., Rankin R.A., 1989. Geology and economic evaluation of the Mt. Weld carbonatite, Laverton, Western Australia. In: Kimberlite and Related Rocks. Geological Society of Australia, Special Publication, 14, 1215-1235.

Xu C., Kynicky J., Chakhmouradian A.R. Campbell I.H., Charlotte M.A., 2010. Trace-element modeling of the magmatic evolutionof rare-earth-rich carbonatite from the Miaoya deposit, central china. Lithos 118, 145-155.

Xu C., Kynicky J., Chakhmouradian A.R., Li X., Song W., 2015. A case example of the importance of multi-analytical approach in deciphering carbonatite petrogenesis in South Qinling orogen: Miaoya rare-metal deposit, central China. Lithos 227, 107-121.

Zaraisky G., Korzhinskaya V., Kotova N., 2010. Experimental studies of Ta_2O_5 and columbite-tantalite solubility in fluoride solutions from 300 to 550 °C and 50 to 100 MPa. Mineralogy and Petrology 99, 287-300.